

PAPER

# Resonant frequency tuning of electroactive polymer membranes via an applied bias voltage

To cite this article: Lin Dong *et al* 2018 *Smart Mater. Struct.* **27** 114005

View the [article online](#) for updates and enhancements.

# Resonant frequency tuning of electroactive polymer membranes via an applied bias voltage

Lin Dong<sup>1</sup>, Michael D Grissom<sup>2</sup>, Tahzib Safwat<sup>3</sup>, M G Prasad<sup>1</sup> and Frank T Fisher<sup>1</sup> 

<sup>1</sup> Department of Mechanical Engineering, Stevens Institute of Technology, Hoboken, NJ 07030, United States of America

<sup>2</sup> KCF Technologies, State College, PA 16801, United States of America

<sup>3</sup> Department of Mechanical Engineering, Pennsylvania State University, University Park, PA 16802, United States of America

E-mail: [Frank.Fisher@stevens.edu](mailto:Frank.Fisher@stevens.edu)

Received 29 March 2018, revised 31 May 2018

Accepted for publication 20 June 2018

Published 25 September 2018



CrossMark

## Abstract

Vibration-based energy harvesting may hold tremendous impact for future applications of continuous machine and structural health monitoring. Here a novel resonant frequency tuning approach is proposed where the application of a bias voltage to a pre-stretched electroactive polymer (EAP) membrane results in changes in membrane tension which can be used to adjust the resonant frequency of the membrane. The effect of the bias voltage on the EAP membrane, which induces an electrostatic pressure and corresponding reduction in membrane thickness, is determined via an analytical model of the activation response of the EAP membrane, with the results confirmed using FEM simulation in ANSYS. Through a mass-loaded circular membrane vibration model, the effective resonant frequency of the membrane can be determined as a function of changes in membrane tension due to the applied bias voltage. In the case of an EAP membrane, pre-stretch contributes to the mechanical stiffness of the system while the applied bias voltage contributes to a change in electrical stiffness of the membrane. Experimental characterization of the EAP material VHB 4910 from 3M verified the resonant frequencies corresponding to the bias voltages predicted from the appropriate models. Given an effective system stiffness range between  $598 \text{ N m}^{-1}$  (when  $\lambda = 1.5$ ,  $U = 0$ ) and  $266 \text{ N m}^{-1}$  (when  $\lambda = 5$ ,  $U = 5000$ ), the corresponding resonant frequency tuning range for a particular circular central loaded EAP membrane device is between 31.4 to 21.8 Hz. The proposed bias voltage tuning approach for the EAP membrane may provide a novel strategy to enable resonant frequency tuning of energy harvesting devices in particular application environments.

Keywords: electroactive polymer, bias voltage, vibration frequency tuning, energy harvesting

(Some figures may appear in colour only in the online journal)

## Nomenclature

		$\zeta_e$	electrical damping ratio
$\alpha$	thermal expansion coefficient	$\zeta_m$	mechanical damping ratio
$\epsilon_0$	free-space ( $8.854 \times 10^{-12} \text{ As V}^{-1} \text{ m}^{-1}$ )	$\zeta_t$	total damping ratio
$\epsilon_r$	dielectric constant	$\lambda$	stretch ratio

$\lambda_{ra}^{II}$	stretch ratio of the active region in the radial direction in state II	$r^I$	membrane radius in a pre-stretched state I
$\lambda_{ta}^{II}$	stretch ratio of the active region in the thickness direction in state II	$r^{II}$	membrane radius in a bias voltage state II
$\lambda_{rb}^{II}$	stretch ratio of the passive region in the radial direction in state II	$r_a^i, c_a^i, t_a^i$	active region (with an electrode) radius, circumference and thickness where superscript $i$ refers to different states of 0, I or II
$\lambda_{tb}^{II}$	stretch ratio of the passive region in the thickness direction in state II	$r_b^i, c_b^i, t_b^i$	passive region (without an electrode) radius, circumference and thickness where superscript $i$ refers to different states of 0, I or II
$\lambda_p$	stretch ratio in a pre-stretch state I	$s_{eff-r}$	effective film stress in the radial direction, which is the [1, 1] element of $[s^{II}][s^{II}]$
$\lambda_r^i, \lambda_c^i, \lambda_t^i$	stretch ratios in the radial, circumferential and thickness directions where superscript $i$ refers to different states of 0, I or II	$s_r^I$	Cauchy stress in the radial direction in state I
$v_t$	nominal actuation strain	$s_z^I$	out-of-plane Cauchy stress in the thickness direction in state I
$\omega_s$	source vibration frequency	$s_{ra}^{II}$	membrane out-of-plane stress after applying the bias voltage
$\omega_{struc}$	undamped natural frequency of the vibrating structure	$s_{ra}^{II}$	membrane in-plane stress after applying the bias voltage
$C_{10}, C_{20}, C_{30}$	unstretched Yeoh model constants	$t^0$	membrane thickness in an initial state 0
$C_{10}', C_{20}', C_{30}'$	stretched Yeoh model constants	$t^I$	membrane radius in a pre-stretched state I
$E$	Young's modulus	$t^{II}$	membrane radius in a bias voltage state II
$I_1$	first invariant Cauchy–Green deformation tensor	$t_a^{II}$	membrane contracted thickness after applying the bias voltage
$M$	mass of the membrane	$[s^I]$	matrix of membrane stress in state I (pre-stretch)
$P$	power output of an energy harvesting device	$[s^{II}]$	matrix of membrane stress in state II (bias voltage)
$P_{res}$	power output at resonance of an energy harvesting device	$[s_E]$	matrix of stress produced by the electrostatic force from the applied bias voltage
$T$	membrane tension		
$T_{eff}$	effective membrane tension		
$U$	applied bias voltage		
$W$	strain energy function $W$ in the Yeoh form		
$Y$	source vibration amplitude		
$a$	radius of the membrane		
$b$	radius of the central added mass		
$b_m$	mechanical damping coefficient		
$b_e$	electrical damping coefficient		
$f_{eff}$	effective system frequency		
$k_{mech}$	mechanical stiffness		
$k_{mech}^I$	membrane mechanical stiffness in state I without consideration of the bias voltage effect		
$k_{elec}$	electrical stiffness		
$k_{eff}$	effective stiffness		
$m$	added mass on the membrane		
$m_{eff}$	effective system stiffness		
$p$	hydrostatic pressure		
$p_{el}$	electrostatic pressure		
$r$	electrode radius ratio		
$r^0$	membrane radius in an initial state 0		

## 1. Introduction

Vibration-based energy harvesting may hold tremendous impact in powering continuous machine and structural health monitoring devices in various application environments, and a comprehensive discussion of vibration-based energy harvesting is available in the literature [1]. Generally, it is desired to ensure that the resonant frequencies of an energy harvesting device match the ambient vibration frequencies to maximize the energy harvested [2]. For example, Challa *et al* [3] presented a resonance frequency tuning approach using a magnetic force applied perpendicular to a cantilever beam, achieving  $\pm 20\%$  of the unturned frequency based on the mode of the magnetic force and the separation distance between the magnets. On the other hand, a horizontal tunable electromagnetic vibration-based micro-generator was designed by Zhu *et al* [4] via induced variable axial magnetic forces. A two-dimensional resonant frequency tuning model was recently developed which generalizes these approaches [5]. The tuning model is based on effective stiffness theory, where the effective resonant frequency of the system is a function of two variable stiffness terms which are in turn governed by the separation of the magnets in 2D space.

**Table 1.** Material parameters of EAP membrane.

Membrane (3M VHB 4910)			
Symbol	Description	Value	Units
$r_0$	Initial radius	19.05	mm
$t_0$	Initial thickness	1000	$\mu\text{m}$
$\lambda$	Stretch ratio	1.1–5	unitless
$\varepsilon_r$	Dielectric constant	4.7	unitless
$E$	Young's modulus	1.44	MPa
$\alpha$	Thermal expansion coefficient	$1.8 \times 10^{-4}$	$\text{m}/\text{m}^\circ\text{C}$
$\varepsilon_{r,\lambda=1}$		4.7	unitless
$\varepsilon_{r,\lambda=1.5}$		4.4	unitless
$\varepsilon_{r,\lambda=3}$	Dielectric constant	3.7	unitless
$\varepsilon_{r,\lambda=4}$		3.2	unitless
$\varepsilon_{r,\lambda=5}$		2.6	unitless
$C_{10}$		0.0693	MPa
$C_{20}$	Unstretched Yeoh model	$-8.8 \times 10^{-4}$	MPa
$C_{30}$		$16.7 \times 10^{-6}$	MPa
$C'_{10}$		0.053 74	MPa
$C'_{20}$	Stretched Yeoh model	$-4.86 \times 10^{-4}$	MPa
$C'_{30}$		$3.89 \times 10^{-6}$	MPa

While cantilever-based energy harvesting geometries have been more frequently studied, membrane-based designs have also been pursued. For example, Rezaeisaray *et al* [6] designed and analyzed an SU-8 membrane-based energy harvester which uses a nonlinear stiffness effect based on a Duffing oscillator to obtain a frequency bandwidth of 146 Hz. Mo *et al* [7] developed a theoretical model for a piezoelectric circular membrane subjected to pressure fluctuations, concluding that the optimization of energy harvesting performance is highly dependent on the ratio between the thickness and radius of the membrane. In addition, a piezoelectric circular membrane array connected in parallel was shown by Wang *et al* [8] to increase the device performance compared to the power generated from a single membrane. Another reported membrane-based energy harvester was proposed by Palosaari [9], whose experimental results suggest that pressure fluctuation could be a potential method to tune the resonant frequency of a membrane-based energy harvester to match the ambient vibrations for maximum power output. Note that the term of *pre-stress* used in [9] refers to the membrane out-of-plane stress, which is different from the usage of the term (denoting membrane in-plane stress) used below in this work. More recently, it was found that mechanical stretch of a hyperelastic polymer membrane induces a membrane tuning stress and corresponding reduction in membrane thickness, which impacts the effective stiffness and hence the vibrational response of the membrane [10]. Membrane geometry-based energy harvesters have become increasingly attractive as a means to leverage the properties of emerging soft materials to target lower frequency vibration sources.

In recent years electroactive polymers (EAPs), which can deform in response to the application of an electrical stimulus, have also been explored for potential mechanical energy harvesting applications [11]. Among EAPs, dielectric elastomers (DEAs) have drawn great attention due to their outstanding overall performance [12], including large elongation, high speed of response, and high energy density. Pelrine [13] proposed DEAs as a means of actuation by using an incompressible DEA membrane between two layers of deposited compliant electrode. When an electric field is applied across the sandwiched membrane, the membrane acts as a capacitor with the Coulombic force generating a Maxwell stress between the electrodes that results in squeezing the DEA membrane and inducing expansion of the DEA due to incompressibility of the elastomer [14]. Typically, silicones or acrylics are used as DEAs, and carbon or graphite powder/grease or other highly compliant metal paints [15] are used as electrodes. The operating voltage of DEAs is around 1–10 kV [16], corresponding to an electric field up to  $100 \text{ V } \mu\text{m}^{-1}$ . In addition, a considerably high actuation strain (over 100%) [17] could also be obtained using DEAs. Several commercial products have been described in the literature such as Polytek Development series poly 74 [17, 18], BJB Enterprise TC-5005 A/B-C silicone [17, 18], Elastosil RT 625 by Wacker [17, 18], Dow Corning HS3 silicone [19], NuSil CF19-218 silicone [19], and 3M VHB 4910 acrylic tapes [19, 20]. Among easy-accessible commercial products [17–20], 3M VHB 4910 acrylic tapes show impressive performance due to the high dielectric constant ( $\varepsilon_r = 4.7$  for an unstretched material) and high actuation strain potential up to 6 times the axial stretch in both planar directions [20] and will be the focus of the work presented here.

Because relatively high actuation strain (over 100%) can be produced through the activation process, DEAs typically demonstrate hyperelastic material behavior, whose stress–strain relationship can be described in terms of a strain energy function. The mechanical behavior of hyperelastic materials have been characterized by different functional forms of the strain energy, such as the commonly used Yeoh [21], Ogden [22] and Mooney–Rivlin [23] models. Previous work found that the membrane thickness decreases in an unstable manner when using the Ogden and Mooney–Rivlin material models, with a corresponding increase in out-of-plane film stiffness not compensating for the increased electrostatic forces [24]. Therefore, the Yeoh form is chosen here for this work to better capture the physical behavior of the EAP material. (The reader is directed to the literature for a more comprehensive discussion of instabilities and failure modes for EAP membranes [25].) In addition, we note that the analytical model described in the next section assumes for simplicity a purely hyperelastic material and neglects more complicated viscoelastic material effects which have been described previously in the literature [26–29].

For a pre-stretched EAP membrane, it has been observed in the literature that the dielectric constant of the VHB elastomer decreases as the stretch ratio is increased [20]. Therefore, changes in the material properties of the VHB membrane as a function of strain may affect the resulting bias voltage

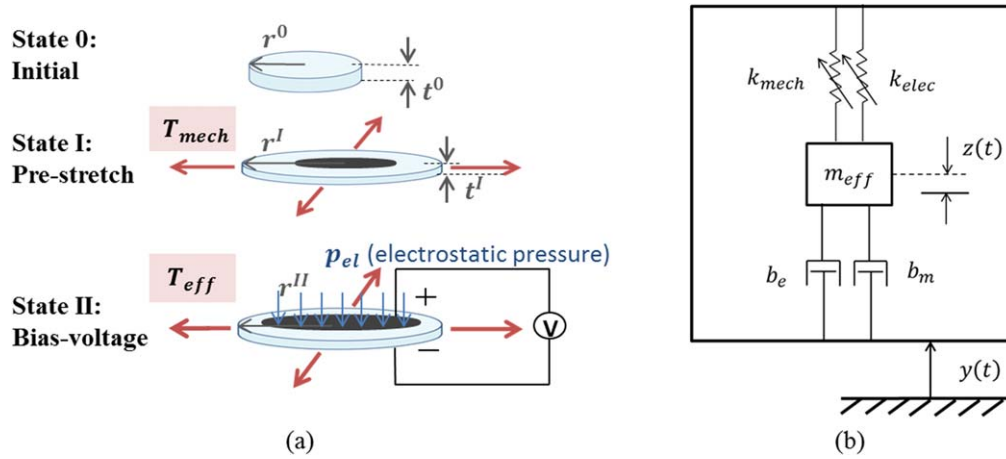


**Figure 1.** (a) Schematic of bias voltage tuning model for pre-stretched circular EAP membrane with three states: 0 (initial), I (pre-stretch), and II (bias voltage).  $T_{mech}$  is the membrane tension in state I only subject to a mechanical stretch, while  $T_{eff}$  is the membrane effective tension in state II as a result of both mechanical and electrical contributions to the membrane tension. (b) Lumped model of the resonant frequency tuning approach where membrane mechanical stiffness and electrical stiffness are represented as variable springs.

response. However, the effect of pre-stretch on the dielectric constant of VHB elastomer is a much debated topic, and complex factors have been proposed to explain the changes of material properties of EAP material due to stretching [30–34]. While a complete explanation for the stretching effect on the changes of EAP material properties is outside the scope of the current work, it appears that those changes can further affect the response of bias voltage activation on the EAP membrane. Therefore, for the membrane material of VHB 4910, the dielectric constants with the stretched Yeoh material model are used in this work. Experimental values of the dielectric constant as well as material properties for the Yeoh model for VHB 4910 material have been measured by Wissler for different pre-stretch levels as listed in table 1 [35] (here  $C_{10}$ ,  $C_{20}$ , and  $C_{30}$  represent the unstretched membrane and  $C_{10}'$ ,  $C_{20}'$  and  $C_{30}'$  describe the stretched membrane material properties, respectively).

## 2. Bias voltage tuning mechanism

In this section, a resonant frequency tuning approach is presented where the application of a bias voltage to a pre-stretched EAP membrane is used to tune the frequency. Here the effective system stiffness (a combination of mechanical and electrical stiffnesses) contributes to the tuned resonant frequencies of the membrane. A general tuning model is first presented following by a discussion of the response of the EAP membrane to a bias voltage and the corresponding change in vibration response due to the induced compressive stress from the applied voltage. Lastly, the impact of membrane mechanical and electrical stiffness contributions on the overall system effective stiffness are highlighted.

### 2.1. EAP membrane tuning via bias voltage

A theoretical lumped parameter tuning model for bias voltage tuning of a pre-stretched membrane-based energy harvester is

shown in figure 1(a). A circular EAP membrane is stretched from the initial state 0 (radius  $r^0$ , thickness  $t^0$ ) to a pre-stretched state I (radius  $r^I$ , thickness  $t^I$ ). (In order to increase the electrical-to-mechanical conversion efficiency, DEAs are commonly pre-stretched up to five times their in-plane dimensions [24].) Afterwards, a bias voltage is applied to the pre-stretched membrane with its active region (electrode coated area) experiencing a further expanded radius and contracted thickness due to the activation of the EAP material while the edge of the membrane is fixed ( $r^I = r^{II}$ ). Therefore, based on the effective stiffness tuning model after both pre-stretch and applied bias voltage activation of the EAP membrane, the effective stiffness of the membrane-based energy harvester is a function of the membrane pre-stretch and bias voltage stiffnesses such that

$$k_{eff} = k_{mech} + k_{elec}, \quad (1)$$

where  $k_{mech}$  and  $k_{elec}$  are mechanical and electrical stiffness, respectively, and an ideal membrane is assumed to have no intrinsic stiffness [36].

An appropriate lumped model for the bias voltage tuning model is shown in figure 1(b). The effective stiffness can be represented as a combination of two parallel variable springs representing mechanical and electrical stiffnesses, while dampers denoted as mechanical dashpot  $b_m$  and electrical dashpot  $b_e$  represent the mechanical losses and the mechanical energy transformed into electrical energy, respectively. The tuned effective frequency  $f_{eff}$  of the EAP membrane-based energy harvester subject to the applied bias voltage can be expressed in equation (2), where  $k_{eff}$  is the effective system stiffness and  $m_{eff}$  is the effective mass of the system.

$$f_{eff} = \frac{1}{2\pi} \sqrt{\frac{k_{eff}}{m_{eff}}} = \frac{1}{2\pi} \sqrt{\frac{k_{mech} + k_{elec}}{m_{eff}}}. \quad (2)$$

While in practice it may be difficult to change the added mass during device operation, an alternative approach highlighted in equation (2) is to adjust the mechanical and electrical stiffnesses of the membrane in order to target the environmental source frequencies. Based on the generic lumped parameter model shown in figure 1(b), the power output of an energy harvesting device given a sinusoidal ambient excitation vibration  $y(t) = Y \sin \omega_s t$  (where  $Y$  and  $\omega_s$  are the source vibration amplitude and frequency, respectively) can be written as [37]

$$P = \frac{m_{\text{eff}} \zeta_t Y^2 \left(\frac{\omega_s}{\omega_{\text{struc}}}\right)^3 \omega_s^3}{\left[1 - \left(\frac{\omega_s}{\omega_{\text{struc}}}\right)^2\right]^2 + \left[2\zeta_t \frac{\omega_s}{\omega_{\text{struc}}}\right]^2}, \quad (3)$$

where the total damping ratio  $\zeta_t$  ( $\zeta_t = \zeta_m + \zeta_e$ ) is the sum of mechanical  $\zeta_m$  and electrical  $\zeta_e$  damping ratios, respectively, and  $\omega_{\text{struc}}$  is the undamped natural frequency of the vibrating structure. Note that the relationship between the damping coefficients of  $b_m$  and  $b_e$  and the unitless damping ratios of  $\zeta_m$  and  $\zeta_e$  used in equation (4) are  $b_m = 2m_{\text{eff}} \zeta_m \omega_{\text{struc}}$  and  $b_e = 2m_{\text{eff}} \zeta_e \omega_{\text{struc}}$ . When the energy harvesting device is in resonance such that  $\omega_s = \omega_{\text{struc}}$ , the power output at resonance  $P_{\text{res}}$  can be simplified as

$$P_{\text{res}} = \frac{m_{\text{eff}} Y^2 \omega_s^3}{4\zeta_t}. \quad (4)$$

## 2.2. Bias voltage activation of EAP membrane

When a bias voltage is applied to a pre-stretched EAP membrane, the membrane further expands in the plane of the membrane and contracts out-of-plane due to the induced electrostatic forces. Here a bias voltage activation model is used to describe the relationship between the applied bias voltage and the resulting EAP membrane stresses and geometry (accounting for electrode area). Note that the following derivations are simplified by assuming the material is incompressible and isotropic such that the stretch ratios in the radial, circumferential, and thickness directions satisfy  $\lambda_r^i \lambda_c^i \lambda_t^i = 1$ , where superscript  $i$  refers to different states of 0, I or II as shown in figure 1(a) and the time dependence of the mechanical response is neglected. Note that the stretch ratios are defined as the ratio of the length of a deformed dimension to the length of the corresponding undeformed dimension. Given that the material is incompressible, the first invariant Cauchy–Green deformation tensor  $I_1$  can be written as  $I_1 = 2\lambda_r^2 + 1/\lambda_r^4$ .

From state 0 to state I, a circular EAP membrane is subjected to a pre-stretch  $\lambda_p$  such that  $\lambda_r^I = \lambda_p$ ,  $\lambda_c^I = \lambda_p$  and  $\lambda_t^I = 1/(\lambda_r^I \lambda_c^I) = 1/\lambda_p^2$ . After pre-stretch, the membrane is activated from state I to state II by applying a bias voltage. As shown in figure 1(a), the electrode area of the EAP membrane is denoted as the active region with radius  $r_a^i$ , circumference  $c_a^i$ , and thickness  $t_a^i$ , while the passive region refers to the outer region of the membrane area without an electrode and has dimensions  $r_b^i$ ,  $c_b^i$  and  $t_b^i$ . Here the nominal

actuation strain  $v_t$  and the electrode radius ratio  $r$  are defined as

$$v_t = \frac{t_a^{II}}{t_a^I} - 1, \quad (5)$$

$$r = \frac{r_a^I}{r^I}. \quad (6)$$

Due to the electroactive response of the EAP material, the stretch ratios of the active and passive region in the radial and thickness directions of the membrane can be determined based on a previously described spring-roll model [24] such that

$$\lambda_{ra}^{II} = \frac{\lambda_r^I}{v_t + 1}, \quad (7)$$

$$\lambda_{ta}^{II} = \frac{v_t + 1}{\lambda_r^I \cdot \lambda_c^I}, \quad (8)$$

$$\lambda_{rb}^{II} = \lambda_r^I \cdot \frac{v_t + 1 - r}{(1 - r)(v_t + 1)}, \quad (9)$$

$$\lambda_{tb}^{II} = \frac{1}{\lambda_r^I \cdot \lambda_c^I} \cdot \frac{(v_t + 1)(1 - r)}{v_t + 1 - r}. \quad (10)$$

Given the definition of  $\lambda_{ra}^{II}$  from equation (8), the contracted thickness in the active region after the application of the bias voltage ( $t_a^{II} = t_a^I \lambda_{ra}^{II}$ ) in state II can be expressed as

$$t_a^{II} = t_a^I \cdot \frac{v_t + 1}{\lambda_r^I \cdot \lambda_c^I}. \quad (11)$$

For an incompressible material, the Cauchy stresses  $s_i$  are defined as the force per unit area of the deformed configuration. They can be determined based on the derivative of the strain energy potential with respect to the stretch ratios  $\lambda_i$  and the hydrostatic pressure  $p$  which enforces the incompressibility constraint [22], where subscript  $i$  refers to the different directions for simplification in the following equations. Thus the Cauchy stress in the radial direction in state I is  $s_r^I = \lambda_r^I \partial W / \partial \lambda_r^I - p$  and the out-of-plane Cauchy stress in the thickness direction in state I is zero due to the assumption of plane stress for a thin membrane ( $s_z^I = \lambda_z^I \partial W / \partial \lambda_z^I - p = 0$ ).

The strain energy function  $W$  in the Yeoh form can be written as  $W = C_{10}'(I_1 - 3) + C_{20}'(I_1 - 3)^2 + C_{30}'(I_1 - 3)^3$  where  $I_1$  is the component of the Cauchy–Green deformation tensor which is a function of stretch ratios as given in [21] and the values of the stretched material parameters ( $C_{10}'$ ,  $C_{20}'$  and  $C_{30}'$ ) are given in table 1. Therefore, the Cauchy stress in the radial direction in state I for a circular EAP membrane-based on the Yeoh model can be written as

$$s_r^I = 2 \cdot \left( \lambda_p^2 - \frac{1}{\lambda_p^4} \right) \cdot [C_{10}' + 2 \cdot C_{20}' \cdot \left( 2\lambda_p^2 + \frac{1}{\lambda_p^4} - 3 \right) + 3 \cdot C_{30}' \cdot \left( 2\lambda_p^2 + \frac{1}{\lambda_p^4} - 3 \right)^2]. \quad (12)$$

Different stretch ratios of  $\lambda_{ra}^{II}$ ,  $\lambda_{ta}^{II}$ ,  $\lambda_{rb}^{II}$ ,  $\lambda_{tb}^{II}$  are determined as a function of nominal actuation strain  $v_t$  using equations (7)–(10), respectively. By assuming there is no buckling or bending of the membrane, the membrane stresses produced by the electrostatic forces are hydrostatic [38]. Therefore, the electrostatic pressure  $p_{el}$  can be written in terms of the applied voltage  $U$  and membrane contracted thickness  $t_a^{II}$  [13], and the corresponding membrane radial stress for the active region in state II due to the bias voltage can be rewritten as

$$p_{el} = -s_{ta}^{II} = \varepsilon_r \cdot \varepsilon_0 \cdot \left( \frac{U}{t_a^{II}} \right)^2, \quad (13)$$

$$s_{ra}^{II} = G(\lambda_{ra}^{II}) - G(\lambda_{ta}^{II}) - p_{el}, \quad (14)$$

where  $\varepsilon_r$  is the EAP dielectric constant,  $\varepsilon_0$  is the free-space permittivity ( $8.854 \times 10^{-12}$  As V<sup>-1</sup> m<sup>-1</sup>), and  $G(\lambda_i)$  is defined as

$$G(\lambda_i) = \lambda_i \cdot \frac{\partial W}{\partial \lambda_i}. \quad (15)$$

Given the boundary condition that the axial forces of the active and passive region are equal for the activation model of the EAP membrane [24], such as  $s_{ra}^{II} c^{II} t_a^{II} = s_{rb}^{II} c^{II} t_b^{II}$ , one can show that

$$G(\lambda_{rb}^{II}) - G(\lambda_{tb}^{II}) = \frac{v_t + 1 - r}{1 - r} \cdot [G(\lambda_{ra}^{II}) - G(\lambda_{ta}^{II}) - p_{el}]. \quad (16)$$

By combining equations (13) and (16), one can derive the final expression for the bias voltage activation model of the pre-stretched EAP membrane in terms of the applied bias voltage  $U$  and the pre-stretch level  $\lambda_p$  as

$$U^2 = \frac{t_0^2}{\varepsilon_r \cdot \varepsilon_0} \cdot \left( \frac{v_t + 1}{\lambda_p^2} \right)^2 \cdot [G(\lambda_{ra}^{II}) - G(\lambda_{ta}^{II}) - \frac{1 - r}{v_t + 1 - r} \cdot (G(\lambda_{rb}^{II}) - G(\lambda_{tb}^{II}))]. \quad (17)$$

According to equation (17), the nominal actuation strain  $v_t$  can first be determined based on the applied bias voltage  $U$ , the pre-stretch level  $\lambda_p$ , and the derivatives of the strain energy function with respect to different stretch ratios (based on equation (15)). From there, the nominal actuation strain  $v_t$  can be further used to calculate the membrane contracted thickness  $t_a^{II}$ , the out-of-plane stress  $s_{ta}^{II}$ , and the radial stress  $s_{ra}^{II}$  of active region based on equations (11), (13) and (14), respectively. It is clear from equation (17) that the activation response of an EAP membrane is a function of the membrane pre-stretch level  $\lambda_p$  and the applied bias voltage  $U$ .

### 2.3. Vibration of a central mass-loaded circular membrane

Now that the membrane activation to a bias voltage has been determined, an analytical model is developed to describe the vibration response of a circular EAP membrane with a centrally-located added mass. By definition, membranes are always stretched in tension. In addition, here only the first fundamental mode, with maximum amplitude at the center, is

considered. For a perfectly clamped homogeneous circular membrane with a centrally loaded mass, the first fundamental frequency can be written as [39]

$$f = \frac{1}{2\pi} \sqrt{\frac{2\pi \cdot T}{m \ln\left(\frac{a}{b}\right)}}. \quad (18)$$

Here we assume that the added mass  $m$  is spread over a contact circle of radius  $b$  at the center of the membrane with a radius of  $a$ . We also assume that the membrane tension  $T$  is much larger than the force applied to the membrane by the added mass  $m$ , such that the effect of the added mass on the tension of the membrane can be neglected. The mass of the membrane  $M$  is assumed small compared to the added mass  $m$  and hence neglected. Note that in the derivation of equation (18),  $b$  must not be significantly smaller than  $a$ , as this concentrated ‘point load’ would result in significant deformation in the center of the membrane [39]. Comparing equation (18) with (2), it is thus straightforward to write the effective mass in equation (2) as  $m_{eff} = m \ln(a/b)$  and the effective stiffness  $k_{eff}$  of the centrally loaded membrane (with no bias voltage) as  $k_{eff} = k_{mech} = 2\pi T$ , respectively.

When a bias voltage is applied to a pre-stretched membrane, the membrane further expands in the radial direction and contracts out-of-plane due to the induced electrostatic forces. This is due to the fact that when the EAP membrane is subjected to a bias voltage, a compressive stress is generated and squeezes the membrane such that the activated region of the membrane seeks to expand in-plane, but the edge of the passive (non-activated, non-electroded) region is clamped, which relaxes the effect of the pre-stress. As proposed in the literature [40], the electrostatic force from an applied voltage adds a compressive stress to the membrane, effectively softening the membrane and reducing its resonant frequency. To simplify the analysis in this section the electrode area (active region) here is assumed to cover the entire membrane. By defining  $[s^I]$  and  $[s_E]$  as the membrane stress in state I (pre-stretch) and the stress produced by the electrostatic force from the applied bias voltage, respectively, the membrane stress in state II (bias voltage)  $[s^{II}]$  can be written as

$$[s^{II}] = [s^I] + [s_E] = \begin{bmatrix} s_r^I + s_E & & \\ & s_c^I + s_E & \\ & & s_t^I + s_E \end{bmatrix}. \quad (19)$$

As has been done previously in the literature, one can assume that there is no buckling or bending of the membrane, thus the electrostatic force must be hydrostatic with only non-zero terms in the diagonal of the stress tensor  $[s_E]$  [38]. Given the electrostatic compressive stress from equation (13), the effective film stress in the radial direction  $s_{eff-r}$ , which is the [1, 1] element of  $[s^{II}]$  in equation (19), can be expressed as

$$s_{eff-r} = s_r^I - \varepsilon_r \cdot \varepsilon_0 \cdot \left( \frac{U}{t_a^{II}} \right)^2. \quad (20)$$

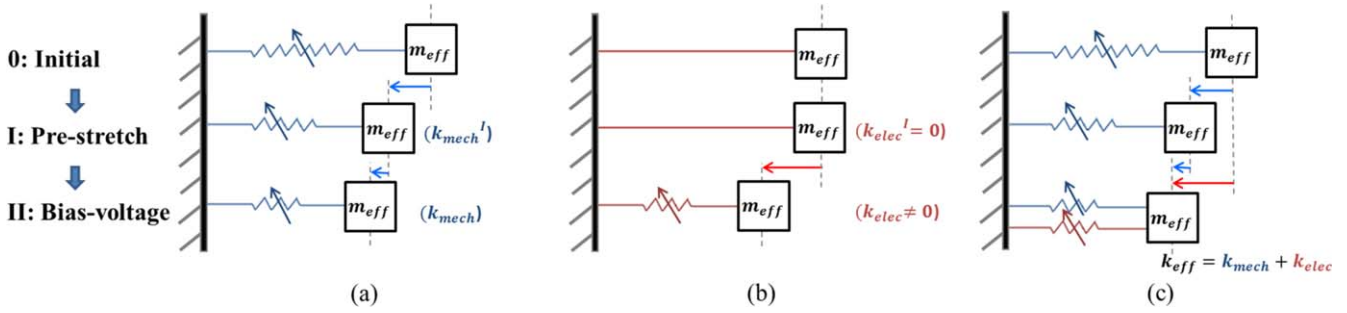


**Figure 2.** Schematic of the resonant frequency tuning mechanism based on the effective stiffness model: (a) mechanical stiffness component; (b) electrical stiffness component; (c) effective system stiffness. The mechanical stiffness and electrical stiffness are represented as springs with variable stiffness.

Because the membrane tension  $T_{eff}$  is the product of the membrane stress  $s_{eff-r}$  and the contracted thickness  $t_a^{II}$  such that  $T_{eff} = s_{eff-r} \cdot t_a^{II}$ , substitution of  $s_{eff-r}$  from equation (20) into (19) yields the frequency of a mass-loaded EAP circular membrane as

$$f_{eff} = \frac{1}{2\pi} \sqrt{\frac{2\pi \left[ s_r^I - \varepsilon_r \cdot \varepsilon_0 \cdot \left( \frac{U}{t_a^{II}} \right)^2 \right] \cdot t_a^{II}}{m \ln\left(\frac{a}{b}\right)}}, \quad (21)$$

where the membrane radial stress  $s_r^I$  resulting from the pre-stretch is determined by the pre-stretch level  $\lambda_p$  while the contracted thickness  $t_a^{II}$  can be calculated by the response of bias voltage activation. Therefore, the resonant frequency  $f_{eff}$  of a pre-stretched centrally loaded circular EAP membrane after application of the bias voltage is a function of both pre-stretch level of  $\lambda_p$  and applied bias voltage  $U$  and can be determined by equation (21).

#### 2.4. Impact of pre-stretch and bias voltage on effective stiffness

Using the resonant frequency tuning approach outlined above, one can derive the mechanical and electrical stiffnesses terms which contribute to the effective system stiffness. These stiffness terms can be adjusted via control of the pre-stretch and the application of a bias voltage, respectively, to implement the overall change in resonant frequency of the EAP membrane. By comparing the vibration model from equation (2) and the tuned frequency of the EAP membrane subject to the applied bias voltage in equation (21), it is straightforward to determine the effective stiffness  $k_{eff}$  as

$$k_{eff} = 2\pi \cdot s_r^I \cdot t_a^{II} - 2\pi \cdot \varepsilon_r \cdot \varepsilon_0 \cdot \frac{U^2}{t_a^{II}}, \quad (22)$$

where the two variable stiffness components representing the mechanical and electrical stiffnesses can be written as

$$k_{mech} = 2\pi \cdot s_r^I \cdot t_a^{II}, \quad (23)$$

$$k_{elec} = -2\pi \cdot \varepsilon_r \cdot \varepsilon_0 \cdot \frac{U^2}{t_a^{II}}. \quad (24)$$

Here the mechanical stiffness refers to the contribution of mechanical stretch, while the electrical stiffness is the result of the applied bias voltage. However, as will be discussed later the application of a bias voltage will also result in a

slight change in the mechanical stiffness. According to equation (24), the change in the membrane mechanical stiffness  $k_{mech}$  is a function of membrane radial stress  $s_r^I$  and contracted thickness  $t_a^{II}$ .

On the other hand,  $k_{mech}^I$  is defined as the membrane mechanical stiffness in state I without consideration of the bias voltage effect, and thus is different from the overall system mechanical stiffness  $k_{mech}$  which includes both pre-stretch and bias voltage effects. By substituting  $s_r^I$  from equation (12) and  $t^I = t^0/\lambda_p^2$  (the membrane contracted thickness in state I due to the pre-stretch) into the expression of  $k_{mech}^I = 2\pi \cdot s_r^I \cdot t^I$ , the membrane mechanical stiffness  $k_{mech}^I$  in state I can be written as

$$k_{mech}^I = 4\pi \cdot t^0 \cdot \left( 1 - \frac{1}{\lambda_p^6} \right) \cdot [C_{10}' + 2C_{20}' \cdot \left( 2\lambda_p^2 + \frac{1}{\lambda_p^4} - 3 \right) + 3C_{30}' \left( 2\lambda_p^2 + \frac{1}{\lambda_p^4} - 3 \right)^2]. \quad (25)$$

When the membrane is subjected to a bias voltage after pre-stretch, the overall system mechanical stiffness  $k_{mech}$  can be determined from equation (23) being sure to take into account the further contracted thickness of the active region  $t_a^{II}$  due to applied bias voltage.

An explanation of the mechanical stiffness component of the resonant frequency tuning mechanism for the membrane is shown schematically in figure 2(a). When the membrane is pre-stretched from initial state 0 to the pre-stretched state I, a variable spring representing the mechanical stiffness  $k_{mech}^I$  compresses with the pre-stretch level. Note that different material parameters contribute to the mechanical stiffness of state I ( $k_{mech}^I$ ) as a function of stretch ratio  $\lambda_p$  based on equation (25). Here a material model using different dielectric constants and stretched Yeoh material constants that are a function of the applied stretch are used in the analysis. After applying a bias voltage the system moves from state I to state II, and the overall mechanical stiffness  $k_{mech}$  further compresses as shown in figure 2(a) due to the decrease in membrane thickness upon the application of the bias voltage.

The electrical stiffness contribution  $k_{elec}$  provided by the applied bias voltage is given by equation (24). As shown in figure 2(b), at zero bias voltage in state I  $k_{elec} = 0$ . On the other hand, in state II the electrostatic force from an applied

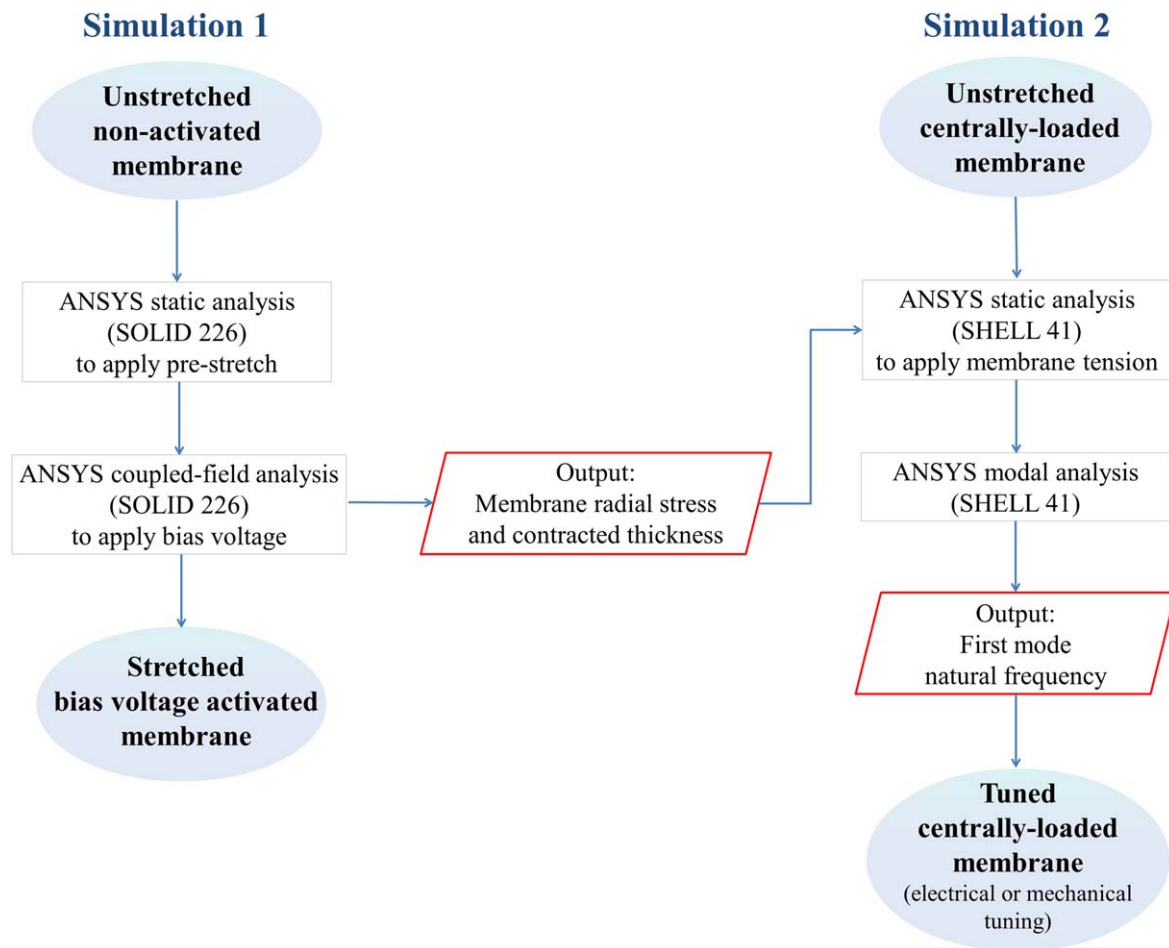


**Figure 3.** Flow chart of finite element modeling using ANSYS for the circular EAP membrane.

voltage adds a compressive stress to the membrane, which contributes a negative electrical stiffness to the system. When both pre-stretch and bias voltage are applied to an EAP membrane, the resonant frequencies are altered as the result of both mechanical stiffness and electrical stiffness contributions as shown in figure 2(c). Calculation and discussion of the mechanical, electrical, and effective system stiffnesses based on this model will be presented in section 5.

### 3. Finite element modeling approach

To verify the analytical results obtained using the expressions above, two separate FEM simulations using ANSYS were performed for the circular EAP membrane as described in this section. In the first analysis using ANSYS (simulation 1), the membrane tuning stresses were first determined as a function of the applied bias voltage to apply the appropriate tension to the membrane. This result then forms the basis for the second FEM step (simulation 2), where a static analysis and a modal analysis are used to determine the resonant frequencies of the central mass-loaded membrane as shown in figure 3.

Schematic models of the ANSYS simulations are shown in figure 4, where an opening angle of  $30^\circ$  and cyclic symmetry in cylinder coordinates are applied. The hyperelastic

membrane (VHB 4910) is modeled using the coupled-field element SOLID 226 with KEYOPT (11) set to 1 to characterize a fully incompressible elastomer. In ANSYS the VHB 4910 material is modeled using a 3rd order reduced polynomial form of the strain energy function in the Yeoh form with values for  $C_{10}'$ ,  $C_{20}'$ , and  $C_{30}'$  listed in table 1. As shown in figure 4(a), in simulation 1 the pre-stretch in ANSYS is first implemented by imposing the displacement of the nodes at the model boundary from initial radius  $r^0$  to a stretched radius  $r^l$  (where  $r^l = \lambda_p r^0$ ). The second step in simulation 1 is to apply a bias voltage on the nodes of the top layer of the membrane as shown in figure 4(b) (the nodes on the bottom layer are set to zero voltage); here an active region (with electrode area) of 80% area of the membrane is assumed and is subjected to the bias voltage. This step of bias voltage activation is solved by a coupled-field analysis with large-deflection (NLGEOM) and stress-stiffening (PSTRES) effects enabled, respectively.

Once the analysis for the membrane radial stress has been completed, this result is then used to determine the resonant frequency of the stretched membrane (with a central proof mass added at this stage) for comparison with the theoretical calculations of membrane tuned frequency. In simulation 2, the membrane with central loaded mass is modeled asymmetrically using ANSYS Shell 41 elements with an opening

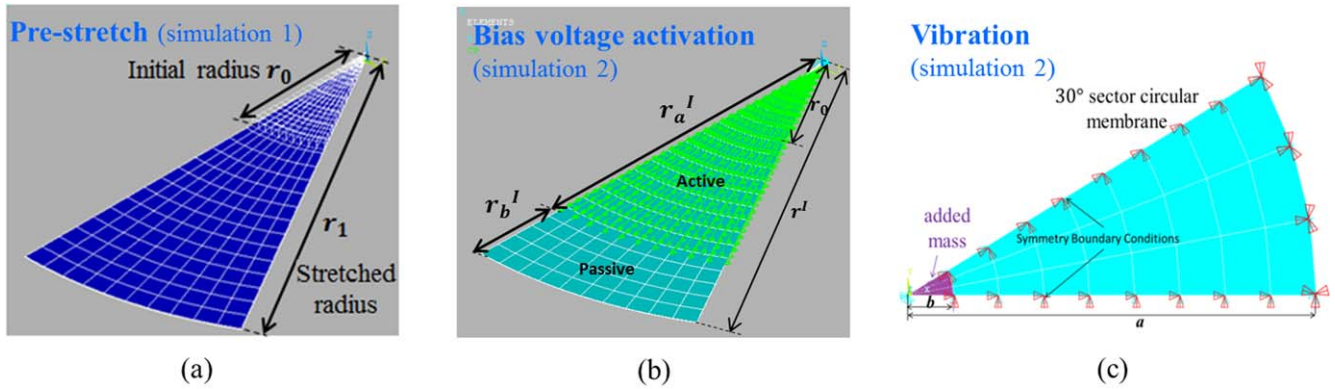


**Figure 4.** ANSYS models of a circular EAP membrane in simulation 1 subjected to (a) pre-stretch and (b) bias voltage activation; (c) a schematic vibration model of a circular membrane with a centrally loaded mass in ANSYS simulation 2.

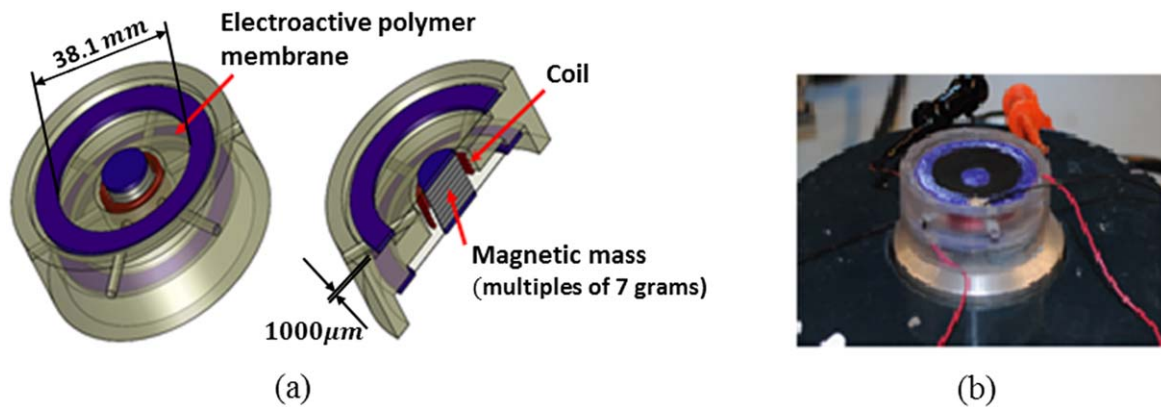


**Figure 5.** (a) Schematic of the resonant frequency test for a circular EAP membrane with a centrally loaded (magnetic) mass. (b) Picture of the prototype mounted to the shaker (Device 1).

angle of  $30^\circ$  and symmetric boundary conditions as shown in figure 4(c). A radius ratio between the membrane and the central load of  $a/b = 9$  was used for the FEM analysis to enable comparison with the experimental study described in the next section. In the analysis for the centrally loaded membrane, a static analysis is first performed to apply the desired tension calculated from the initial FEM analysis as a function of the stretch ratio [41]. Specifically, this membrane stress is induced by the method of uniform cooling, where the temperature difference  $\Delta T_{temp}$  is calculated from  $\Delta T_{temp} = T/(E\alpha t)$  [42], where  $T$  is the tension of the membrane and  $E$  and  $\alpha$  are the Young's modulus and thermal expansion coefficient of the membrane, respectively. Details of the parameters used in the ANSYS study are given in table 1. The next step in simulation 2 is the modal analysis of the clamped membrane with the added central mass. Here the added mass attached to the central section of the membrane is modeled as two sets of overlapping elements, where the first set of elements representing the membrane (lower layer) has its nodal plane located on the 'top' face, whereas the set of elements corresponding to the added mass (top layer) has its nodal plane located on the 'bottom' face. The tuned membrane frequencies determined based on this FEM approach will be compared with both analytical predictions and experimental studies in section 5.

#### 4. Experimental methods

In this section, two separate prototype devices denoted as Devices 1 and 2, respectively, are tested to determine the effective resonant frequencies of the membranes. An initial experimental study (Device 1) measuring the resonant frequency of a mass-loaded circular EAP membrane as a function of mechanical stretch and applied bias voltage was first conducted to confirm the analytical and computational models described above. The membrane material used here is 3M VHB 4910 acrylic with material properties given in table 1. A  $1000 \mu\text{m}$  thick (initial thickness) commercially available membrane was pre-stretched to a membrane thickness of  $60 \mu\text{m}$  in this initial experiment (Device 1). The tests to determine the resonant frequencies of the membranes were performed by mounting a prototype on a shaker (Vibration Test Systems VG-100A-6) to evaluate the frequency of the mechanism as shown in figure 5. The prototype consisted of a membrane, a central magnet/mass, and a coil fixed to the frame; this prototype is then mounted on the shaker to provide a given vibration of known amplitude and frequency. A 7 g ferrous mass was added at the center of the membrane. The resonance for the mass-membrane system was evaluated by measuring the frequency response function of the voltage induced in the coil relative to the input force measured by a dynamic load cell (PCB 208A02) mounted between the

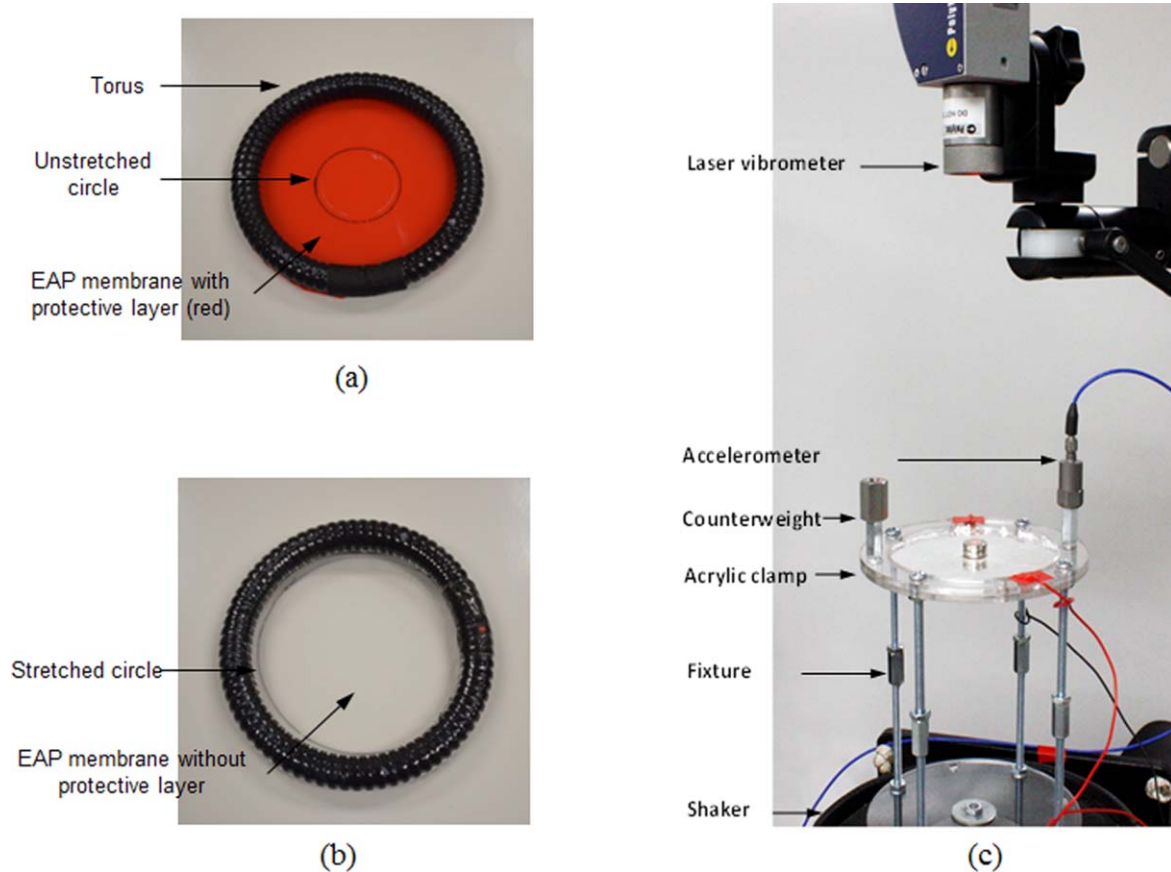


**Figure 6.** (a) Unstretched circular EAP membrane; (b) stretched circular EAP membrane; (c) picture of the prototype mounted to the shaker for additional experimental test (Device 2).

shaker and the prototype using a high impedance measurement device (NI-9215). The peak of the frequency response function is measured for a range of bias voltages spanning 0–4600 V to estimate the resonance frequency of the system. The maximum applied voltage of 4600 V corresponds to an electrical field of  $76.7 \text{ V } \mu\text{m}^{-1}$ , which will not exceed the EAP material electrical breakdown field of  $100 \text{ V } \mu\text{m}^{-1}$  [16].

Furthermore, additional experimental validation (referred to as Device 2) was performed using the test setup shown in figure 6. In this additional set of experiments, a 3M VHB 4910 EAP membrane with the initial thickness of  $1000 \mu\text{m}$  was radially pre-stretched to a thickness of  $40 \mu\text{m}$  using a turnable torus with a rigid core as shown in figures 6(a) and (b). Silver leaf was applied to both sides of the membrane as the electrode. As shown in figure 6(c), two ring acrylic disks were used to clamp the stretched EAP membrane, and each disk fixture was attached to a small piece of conductive copper tape across the thickness of the inner diameter for wire connections. The tests to determine the resonant frequencies of the membranes were performed by mounting the prototype on a shaker (Vibration Test Systems VG-100A-6). As shown in figure 6(c), the fixture was made high enough to keep the EAP membrane with central loaded mass outside of the magnetic field of the shaker, while a counterweight on the clamp was used to reduce the bending mode vibration caused by the eccentric placement of the accelerometer (PCB 353B02) measuring the motion of the clamp. Tests were

conducted by adding multiples of 2.75 g magnetic masses (Magcraft NSN0590) to the center of the EAP membrane under a bias voltage sweep from 0 to 3000 V, corresponding to a maximum of electrical field of  $75 \text{ V } \mu\text{m}^{-1}$ . The output deflection of the centrally loaded EAP membrane was measured at the center of the magnetic mass using a laser vibrometer (OFV-534/5000) as a function of a frequency sweep from the shaker between 0 and 100 Hz. In this experiment, a power amplifier (Trek 609E-6) supplied the bias voltage. The equipment was controlled via LabVIEW with a data acquisition system (National Instruments USB-6343). The test was run three times with the average result reported.

## 5. Results and discussion

Based on the bias voltage frequency tuning mechanism described above, an EAP membrane can be tuned by changing the system effective stiffness, which is comprised of both mechanical and electrical stiffness components. The results for the membrane stresses (both in-plane and out-of-plane) of the electroded active region and the corresponding membrane contracted thickness due to the bias voltage activation are discussed in this section, after which the effective stiffness and the corresponding tuning frequencies are presented.

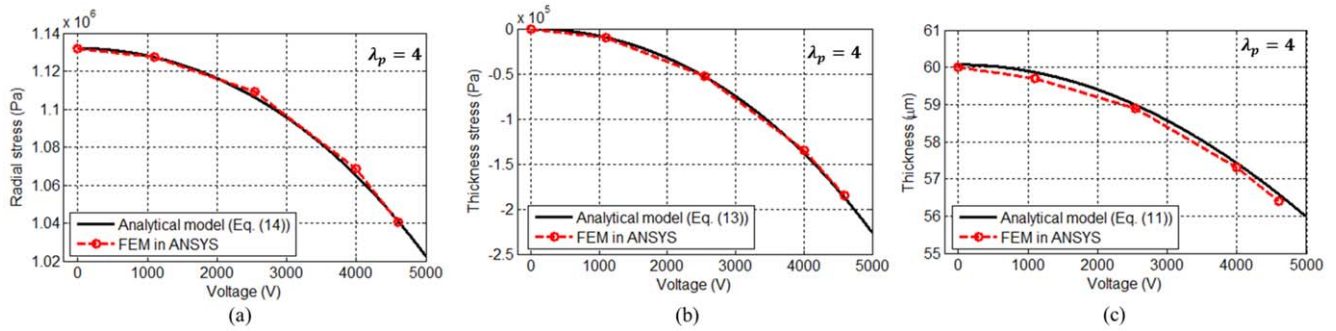


**Figure 7.** EAP membrane response to a bias voltage activation at a pre-stretch  $\lambda_p = 4$ , where the stretch ratio  $\lambda_p$  is defined as the ratio of a stretched radius to initial radius ( $\lambda_p = r^I/r^0$ ): (a) membrane stresses in radial direction; (b) membrane stresses in thickness direction; and (c) membrane contracted thickness.

### 5.1. Membrane tuning stresses and contracted thickness

The response of the EAP membrane to an applied bias voltage at a pre-stretch of  $\lambda_p = 4$  is shown in figure 7, which includes the theoretical and FEM results for the membrane radial stress, thickness stress, and corresponding membrane contracted thickness in the active region. The dimension as well as material properties for the EAP membrane have been listed in table 1. Given that the limit of the electrical field on the material of VHB 4910 used in this work is  $100 \text{ V } \mu\text{m}^{-1}$  [15], maximum applied voltages of 4600 V for Device 1 (stretched film thickness of  $60 \text{ } \mu\text{m}$ ) and 3000 V for Device 2 (stretched film thickness of  $40 \text{ } \mu\text{m}$ ) are used, respectively. From figure 7 it is clear that FEM results (symbols) agree well with the theoretical calculations performed by MATLAB. Here the results from the FEM analysis are the average values of the membrane stresses (in both radial and thickness directions) for nodes in the active region. The scatter of the stresses and membrane thickness values from FEM were generally found to be within 0.02% and 0.04%, respectively. Note that both approaches use the stretched material model, with the membrane material properties in the Yeoh form [ $C_{10}'$ ,  $C_{20}'$  and  $C_{30}'$ ] with different dielectric constants listed in table 1. From figure 7(a), the membrane radial stress in the active region decreases with increasing applied voltage because when the membrane is subjected to a pre-stretch, the activated region of the membrane seeks to expand in-plane, but the edge of the passive (non-activated, non-electroded) region is clamped, which relaxes the effect of the pre-stress. However, note that this in-plane expansion due to activation is small compared with the pre-stretch elongation, and thus the changes in the membrane radial stress with the applied bias voltage shown in figure 7(a) are relatively small.

On the other hand, the applied bias voltage induces an electrostatic pressure  $p_{el}$  corresponding to a negative value for the membrane out-of-plane stress  $s_{ta}^{II}$  in the active region (see equation (13)), decreasing to  $-2.26 \times 10^5 \text{ Pa}$  with an applied bias voltage of up to 5000 V as shown in figure 7(b). Again the FEM results (symbols) agree well with the theoretical calculations (solid lines). In addition, the theoretical result for the membrane contracted thickness  $t_a^{II}$  based on equation (11) where the nominal actuation strain for a given bias voltage is found via equation (17), is given in figure 7(c)

and shows that the membrane thickness decreases from  $60 \text{ } \mu\text{m}$  at zero voltage down to  $55.9 \text{ } \mu\text{m}$  with applied bias voltage of 5000 V. Here the results from the FEM analysis are the average values of displacement differences between the membrane top and bottom layers for the activated nodes of the membrane.

### 5.2. Effective system stiffness

When both pre-stretch and bias voltage are applied to a circular EAP membrane, the resonant frequencies are altered as a function of both the mechanical stiffness  $k_{mech}$  and electrical stiffness  $k_{elec}$  contributions to the overall effective stiffness  $k_{eff}$  of the system (equation (1)). According to equation (25), the pre-stretch level  $\lambda_p$  and material properties [ $C_{10}'$ ,  $C_{20}'$ ,  $C_{30}'$ ] affect the mechanical stiffness in state I ( $k_{mech}^I$ ) when the bias voltage is equal to zero. Figure 8(a) first presents the overall mechanical stiffness as a function of bias voltage for different levels of pre-stretch  $\lambda_p$  using equation (24). Here the mechanical stiffness of the membrane decreases with an increase of the membrane stretch ratio. For sake of comparison, the mechanical stiffness in state I ( $k_{mech}^I$ ) when a circular EAP membrane is only subjected to a stretch (zero bias voltage) is represented by a dashed line in figure 8(a). The results show that the mechanical stiffness in state I ( $k_{mech}^I$ ) decreases at a faster rate for stretch ratios between 2.5 and 4 which is due to the changing material properties of the stretched VHB material. The results shown in figure 8(a) indicate that while the mechanical stretch determines the membrane mechanical stiffness in state I ( $k_{mech}^I$ ), the applied bias voltage contributes a softening effect on the overall membrane mechanical stiffness ( $k_{mech}$ ) component.

To illustrate the impact of membrane pre-stretch on the overall mechanical stiffness, a plot of normalized mechanical stiffness as a function of bias voltage is shown in figure 8(b), where the normalized term is defined as the ratio of the overall membrane mechanical stiffness versus the mechanical stiffness at zero voltage. As shown in figure 8(b), the normalized membrane mechanical stiffness decreases faster at larger stretch ratios. The decrease of the mechanical stiffness with increasing stretch ratios for the EAP membrane is due to the changing material properties of the stretched VHB

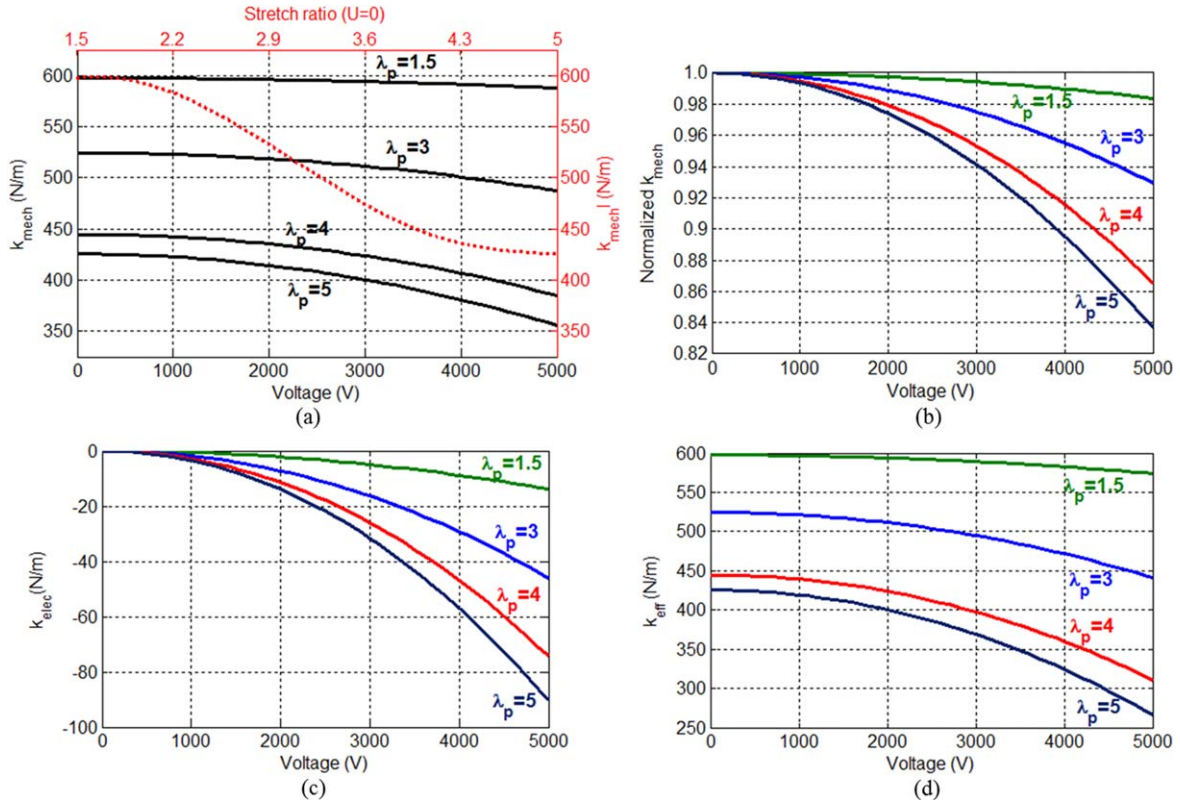


**Figure 8.** Membrane stiffnesses for different pre-stretch levels, where the stretch ratio  $\lambda_p$  is defined as the ratio of a stretched radius to initial radius ( $\lambda_p = r^l/r^0$ ): (a) mechanical stiffness with and without applied bias voltage; (b) normalized membrane mechanical stiffness as a function bias voltage; (c) electrical stiffness component; (d) effective system stiffness.

material. From figure 8(b), the normalized mechanical stiffness at a lower pre-stretch level ( $\lambda_p = 1.5$ ) is in general relatively small and thus will not drastically shift the resonance of the membrane. However, at larger pre-stretch levels (i.e.  $\lambda_p = 5$ ), figure 8(b) shows that a 17% change in normalized membrane stiffness can be achieved with an applied bias voltage of 5000 V. This implies that the bias voltage has a more drastic softening effect on the membrane mechanical stiffness at larger pre-stretch levels, suggesting that a large stretch ratio may be desired in order to widen the frequency tuning range available upon the application of the bias voltage.

Theoretical calculations of the membrane electrical stiffness as a function of bias voltage based on equation (24) are shown in figure 8(c). Here one can see that the electrical stiffness  $k_{elec}$  is always negative such that  $k_{elec} < 0$ , further contributing to a decrease of the membrane effective stiffness according to equation (1). Such a result is due to the fact that the electrostatic force from an applied voltage adds a compressive stress to the membrane, and thus softens the effective system stiffness. In addition, figure 8(c) also illustrates that larger pre-stretch levels significantly reduce the electrical stiffness for a given bias voltage.

Furthermore, by combining the results of the membrane mechanical and electrical stiffnesses from figures 8(a) and (c), the effective system stiffness  $k_{eff}$  as a function of bias voltage for different pre-stretch levels can be calculated as shown in figure 8(d). Again, the effective stiffness of the membrane

decreases with an increase in stretch ratio, and further decreases with increasing applied bias voltage for each pre-stretch level. Figure 8(d) shows that an effective system stiffness between  $598 \text{ N m}^{-1}$  (when  $\lambda_p = 4$ ,  $U = 0$ ) and  $266 \text{ N m}^{-1}$  (when  $\lambda_p = 5$ ,  $U = 4600$ ) can be obtained. One can also conclude from figure 8(d) that the effects of the pre-stretch is in general significantly larger than the bias voltage contribution to the system overall effective stiffness term, suggesting that from a tuning perspective it may be possible to use the mechanical and electrical stiffness contributions for coarse and fine frequency tuning, respectively.

### 5.3. Tuned membrane frequency

Based on the applied bias voltage tuning mechanism for the circular EAP membrane described in section 2, the tuned resonant frequency can be determined by equation (2) given the system effective stiffness  $k_{eff}$  (based on equation (22)) and the effective mass  $m_{eff}$  (where  $m_{eff} = m \ln(a/b)$ ). When the effective mass is a constant, the tuned resonant frequency of the membrane is a function of both mechanical and electrical stiffness components and follows a square root relationship with respect to the effective stiffness (similar to the behavior as the effective stiffness  $k_{eff}$  shown in figure 8(d)). A corresponding resonant frequency tuning range for the circular central loaded EAP membrane from 21.8 to 31.4 Hz is observed as shown in figure 9(a). In addition, the results in figure 9(a) show that the resonant frequency of the system at a

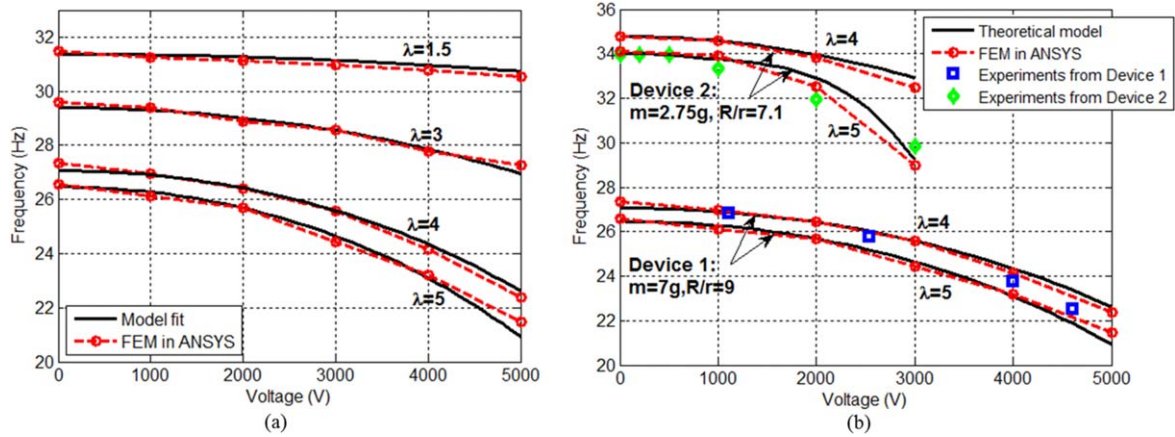


**Figure 9.** The effective first mode natural frequency of a circular mass-loaded EAP membrane as a function of applied bias voltage: (a) comparison of theoretical and FEM simulation subject to different stretch ratios; (b) comparison of analytical prediction and experimental data subject to two separate experiments (Devices 1 and 2).

low pre-stretch level ( $\lambda_p = 1.5$ ) does not experience a significant change in frequency with the applied bias voltage, whereas much more significant frequency shifts are observed at larger stretch ratios (for example,  $\lambda_p = 4$  and  $\lambda_p = 5$ ). This again suggests that a large initial stretch ratio will lead to a more significant tuning range with the application of the bias voltage.

Furthermore, figure 9(b) compares the analytical predictions for the effective resonant frequency of a mass-loaded circular EAP membrane (3M VHB 4910) as a function of bias voltage using equation (21) with two sets of experimental data for Devices 1 and 2 as discussed in section 4. For Device 1, an initial film  $1000 \mu\text{m}$  thick is stretched to a thickness of  $60 \mu\text{m}$  in pre-stretch state I. A  $7 \text{ g}$  magnetic ring mass was then placed at the center of the stretched EAP membrane. A radius ratio of  $R/r = 9$  matching the experimental conditions was used for the analytical predictions. On the other hand, for Device 2, an initial film  $1000 \mu\text{m}$  thick EAP membrane is pre-stretched to a thickness of  $40 \mu\text{m}$ , the radius ratio between membrane and added mass is  $R/r = 7.1$ , and a  $2.75 \text{ g}$  magnetic mass (Magcraft NSN0590) is applied to the center of the stretched EAP membrane. It is clear from figure 9(b) that the theoretical tuning model agrees well with the experimental data observed for each device.

In addition, for purpose of illustration, the transient vibration response for the mass-loaded EAP membrane for Device 2 is shown in figure 10 for different magnitudes of applied bias voltage. It is clear from figure 10 that the effective first mode natural frequency of the circular mass-loaded EAP membrane shifts from  $33.9 \text{ Hz}$  at zero voltage to  $29.8 \text{ Hz}$  at  $U = 3000 \text{ V}$ , consistent with the results shown in figure 9(b).

Lastly, additional tests were performed with Device 2 by adding multiples of  $2.75 \text{ g}$  magnetic masses to the center of the EAP membrane. The experimental frequency results are compared with analytical calculations as a function of the magnitude of the added mass for two applied bias voltages of  $U = 1000 \text{ V}$  and  $U = 3000 \text{ V}$  as shown in figure 11. Clearly, a larger centrally loaded mass can significantly decrease the first natural frequency of the loaded membrane. From

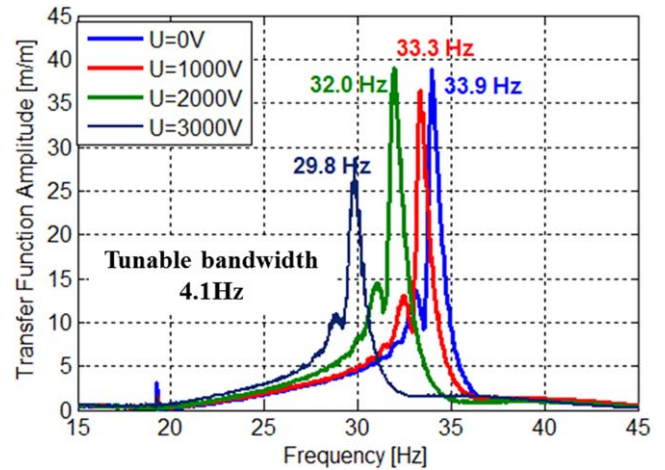


**Figure 10.** Transient vibration response for the mass-loaded EAP membrane from Device 2 for different levels of applied bias voltage.

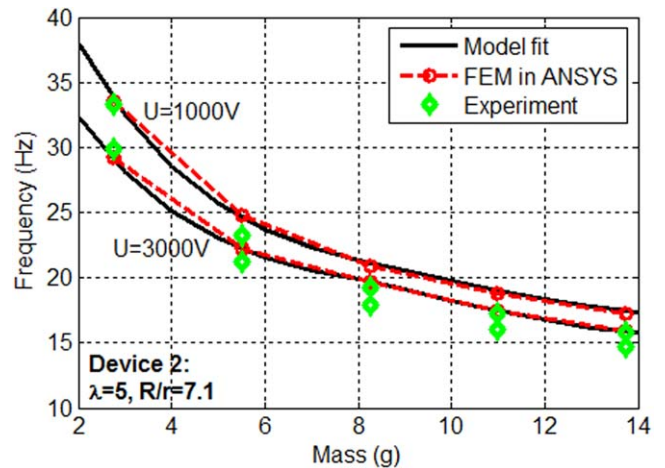


**Figure 11.** Comparison of analytical predictions, experimental data and FEM results for the effective first mode natural frequency of a circular mass-loaded EAP membrane as a function of added mass for two different bias voltages.

figure 11, the experimentally obtained frequencies in most cases closely match the analytical model, with the largest differences found for the cases of more added mass. This error is attributed to the fact that, for larger values of the added mass, the force induced by the added mass may impact the tension of the membrane [41].

As mentioned in section 4, the maximum applied voltage of 4600 V corresponds to an electrical field of  $76.7 \text{ V } \mu\text{m}^{-1}$ , which is less than the electrical breakdown field of  $100 \text{ V } \mu\text{m}^{-1}$  for this EAP material [16]. From a practical perspective, the implementation of a vibration energy harvesting device using a bias voltage tuning approach will need to successfully overcome the challenges of the high voltages needed for actuation. However, the tuning approach may be adapted to additional applications outside of energy harvesting where such voltages are not as challenging to implement. In addition, when considering the long-term system performance of an energy harvester, while the vibration source itself may have an infinite lifetime, the lifetime of the energy harvester itself will be finite due to material failure, system fatigue, and other considerations. For example, Plante proposed and analyzed three failure criteria based on a DEA actuation model that included material strength failure, dielectric strength failure, and pull-in instability failure, where failure maps were proposed to analyze and predict the failure behavior of the actuator [25]. Characterization of the long-term performance of such devices will be the subject of future work.

## 6. Conclusions

In the current research, a resonant frequency tuning approach for a circular EAP membrane is developed. A pre-stretched EAP membrane subjected to a bias voltage results in changes to both mechanical and electrical stiffness components of the effective stiffness of the system. Specifically, a model which accounts for the change in EAP properties as a function of stretch with various dielectric constants is used due to effect of pre-stretch on the material properties. The predictions for effective resonant frequency of the EAP membrane-based on the analytical model agree well with the two experimental studies. These results suggest the possibility of using the proposed bias voltage approach for EAP membrane-based energy harvesting, and indicate that from a tuning perspective, it might be possible to use the mechanical and electrical stiffness effects for coarse and fine frequency tuning, respectively. We note that a limitation of the proposed bias voltage tuning approach is the high voltages that may be needed for tuning, which may significantly limit the types of applications where such an approach may be practical. However, future work towards a functional prototype using this technology may explore and optimize both the EAP material and electrode patterns to allow actuation and tuning at lower bias voltages. In addition, this approach could also find use in other applications where the tuning of the vibration response of EAP membranes is desired.

## Acknowledgments

This work was supported in part by the Defense Threat Reduction Agency (contract # HDTRA1-11-P-0023). The authors also acknowledge the financial support of the Innovation and Entrepreneurship Doctoral Fellowship program at Stevens.

## ORCID iDs

Frank T Fisher  <https://orcid.org/0000-0003-4476-5040>

## References

- [1] Beeby S P, Tudor M J and White N M 2006 Energy harvesting vibration sources for microsystems applications *Meas. Sci. Technol.* **17** R175–95
- [2] Zhu D, Tudor M J and Beeby S P 2010 Strategies for increasing the operating frequency range of vibration energy harvesters: a review *Meas. Sci. Technol.* **21** 022001
- [3] Challa V R, Prasad M G, Shi Y and Fisher F T 2008 A vibration energy harvesting device with bidirectional resonance frequency tunability *Smart Mater. Struct.* **17** 015035
- [4] Zhu D, Roberts S, Tudor M J and Beeby S P 2010 Design and experimental characterization of a tunable vibration-based electromagnetic micro-generator *Sensors Actuators A* **158** 284–93
- [5] Dong L, Prasad M G and Fisher F T 2016 Two-dimensional resonance frequency tuning approach for vibration-based energy harvesting *Smart Mater. Struct.* **25** 065019
- [6] Rezaeisaray M, Gowini M E, Sameoto D, Raboud D and Moussa W 2015 Wide-bandwidth piezoelectric energy harvester with polymeric structure *J. Micromech. Microeng.* **25** 015018
- [7] Mo C, Davidson J and Clark W W 2014 Energy harvesting with piezoelectric circular membrane under pressure loading *Smart Mater. Struct.* **23** 045005
- [8] Wang W, Yang T, Chen X and Yao X 2012 Vibration energy harvesting using a piezoelectric circular diaphragm array *IEEE Trans. Ultrason. Ferroelectr. Freq. Control* **59** 2022–6
- [9] Palosaari J, Leinonen M, Juuti J, Hannu J and Jantunen H 2014 Piezoelectric circular diaphragm with mechanically induced pre-stress for energy harvesting *Smart Mater. Struct.* **23** 085025
- [10] Dong L, Grissom M, Prasad M G and Fisher F T 2016 Application of mechanical stretch to tune the resonance frequency of hyperelastic membrane-based energy harvesters *Sensors Actuators A* **252** 165–73
- [11] Kornbluh R D *et al* 2013 Stretching the capabilities of energy harvesting: electroactive polymers based on dielectric elastomers *Advances in Energy Harvesting Methods* ed N Elvin and A Erturk (New York, NY: Springer New York) pp 399–415
- [12] Bar-Cohen Y 2004 *Electroactive Polymer (EAP) Actuators as Artificial Muscles: Reality, Potential, and Challenges* (Washington: SPIE Press)
- [13] Pelrine R E, Kornbluh R D and Joseph J P 1998 Electrostriction of polymer dielectrics with compliant electrodes as a means of actuation *Sensors Actuators A* **64** 77–85

- [14] Roentgen W C 1880 About the changes in shape and volume of dielectrics caused by electricity *Ann. Phys. Chem.* **11** 771–86
- [15] Kim K J and Tadokoro S 2007 *Electroactive Polymers for Robotic Applications: Artificial Muscles and Sensors* (London: Springer)
- [16] Pelrine R, Kornbluh R, Pei Q and Joseph J 2000 High-speed electrically actuated elastomers with strain greater than 100% *Science* **287** 836–9
- [17] Gallone G, Galantini F and Carpi F 2010 Perspectives for new dielectric elastomers with improved electromechanical actuation performance: composites versus blends *Polym. Int.* **59** 400–6
- [18] Benslimane M Y, Kiil H-E and Tryson M J 2010 Dielectric electro-active polymer push actuators: performance and challenges *Polym. Int.* **59** 415–21
- [19] Kornbluh R D et al 2002 Electroelastomers: applications of dielectric elastomer transducers for actuation, generation, and smart structures *Proc. SPIE* **4698** 254–70
- [20] Kofod G 2001 Dielectric elastomer actuators *PhD Thesis* Technical University of Denmark, Kongens Lyngby, Denmark
- [21] Yeoh O H 1990 Characterization of elastic properties of carbon-black-filled rubber vulcanizates *Rubber Chem. Technol.* **63** 792–805
- [22] Ogden R W 1972 Large deformation isotropic elasticity: on the correlation of theory and experiment for compressible rubberlike solids *Proc. R. Soc. A* **328** 567–83
- [23] Mooney M 1940 A theory of large elastic deformation *J. Appl. Phys.* **11** 582–892
- [24] Wissler M and Mazza E 2005 Modeling of a pre-strained circular actuator made of dielectric elastomers *Sensors Actuators A* **120** 184–92
- [25] Plante J S and Dubowsky S 2006 Large-scale failure modes of dielectric elastomer actuators *Int. J. Solids Struct.* **43** 7727–51
- [26] Suo Z, Zhao X and Greene W H 2008 A nonlinear field theory of deformable dielectrics *J. Mech. Phys. Solids* **56** 467–86
- [27] Park H S and Nguyen T D 2013 Viscoelastic effects on electromechanical instabilities in dielectric elastomers *Soft Matter* **9** 1031–42
- [28] Zhou J, Jiang L and Khayat R E 2014 Viscoelastic effects on frequency tuning of a dielectric elastomer membrane resonator *J. Appl. Phys.* **115** 124106
- [29] Ask A, Menzel A and Ristinmaa M 2015 Modelling of viscoelastic dielectric elastomers with deformation dependent electric properties *Proc. IUTAM* **12** 134–44
- [30] Vu-Cong T, Jean-Mistral C and Sylvestre A 2012 Impact of the nature of the compliant electrodes on the dielectric constant of acrylic and silicone electroactive polymers *Smart Mater. Struct.* **21** 105036
- [31] Ikeda Y et al 2007 Strain-induced crystallization of peroxide-crosslinked natural rubber *Polymer* **48** 1171–5
- [32] Zhao X and Suo Z 2008 Electrostriction in elastic dielectrics undergoing large deformation *J. Appl. Phys.* **104** 123530
- [33] Diaz-Calleja R and Riande E 2013 Comments on the influence of stretching on the permittivity of dielectric elastomers *Smart Mater. Struct.* **22** 038001
- [34] Vu-Cong T, Nguyen-Thi N, Jean-Mistral C and Sylvestre A 2014 How does static stretching decrease the dielectric constant of VHB 4910 elastomer? *Proc. SPIE* **9056** 90561P
- [35] Wissler M T 2007 Modeling dielectric elastomer actuators *PhD Thesis* Swiss Federal Institute of Technology, Zurich, Switzerland
- [36] Fletcher N H and Rossing T D 1998 *The Physics of Musical Instruments* (New York, NY: Springer)
- [37] Williams C B and Yates R B 1996 Analysis of a micro-electric generator for microsystems *Sensors Actuators A* **52** 8–11
- [38] Popov E P 1968 *Introduction to Mechanics of Solids* (Englewood Cliffs, NJ: Prentice-Hall)
- [39] Fletcher N H 1992 *Acoustic Systems in Biology* (New York, NY: Oxford University Press, Inc.)
- [40] Dubois P, Rosset S, Niklaus M, Dadras M and Shea H 2008 Voltage control of the resonance frequency of dielectric electroactive polymer (DEAP) membranes *J. Microelectromech. Syst.* **17** 1072–81
- [41] Dong L, Grissom M and Fisher F T 2015 Resonant frequency of mass-loaded membranes for vibration energy harvesting applications *AIMS Energy* **3** 344–59
- [42] Timoshenko S and Young D H 1955 *Vibration Problems in Engineering* 3rd edn (New York, NY: D. Van Nostrand Co., Inc)